ChemPubSoc Europe

DOI: 10.1002/chem.201404088

CHEMISTRY A European Journal Full Paper

Oxidation

# Oxygenation by Ruthenium Monosubstituted Polyoxotungstates in Aqueous Solution: Experimental and Computational Dissection of a Ru(III)–Ru(V) Catalytic Cycle

Andrea Sartorel,[a] Pere Miró,[b] Mauro Carraro,[a] Serena Berardi,[a] Olga Bortolini,[c] Alessandro Bagno,[a] Carles Bo,*[b, d] and Marcella Bonchio*[a]

**Abstract:** Molecular polyoxometalates with one embedded ruthenium center, with general formula $[Ru^{II/III}(DMSO)XW_{11}O_{39}]^{n-}$ (X = P, Si; $n$ = 4–6), are readily synthesized in gram scale under microwave irradiation by a flash hydrothermal protocol. These nanodimensional and polyanionic complexes enable aerobic oxygenation in water. Catalytic oxygen transfer to dimethylsulfoxide (DMSO) yielding the corresponding sulfone ($DMSO_2$) has been investigated with a combined kinetic, spectroscopic and computational approach addressing: (i) the $Ru^{III}$ catalyst resting state; (ii) the bimolecular event dictating its transformation in the rate-determining step; (iii) its aerobic evolution to a high-valent ruthenium oxene species; (iv) the terminal fate to diamagnetic dimers. This pathway is reminiscent of natural heme systems and of bioinspired artificial porphyrins. The in silico characterization of a key bis-Ru(IV)-μ-peroxo-POM dimeric intermediate has been accessed by density functional theory. This observation indicates a new landmark for tracing POM-based manifolds for multiredox oxygen reduction/activation, where metal-centered oxygenated species play a pivotal role.

## Introduction

The activation of molecular oxygen by metal complexes for green and selective chemical oxidations remains a formidable challenge and a major goal of the current research activity dedicated to oxidative transformations.[1,2] In particular, there is a call for highly stable oxygenation catalysts, performing ideally in water, under mild temperature and pressure conditions. This quest for such "Holy Grail" of oxidation catalysis finds a unique paradigm within the dioxygenase activity of natural metallo-enzymes,[3,4] which thus provide the functional archetype for the invention of bio-inspired synthetic systems.[5–8] In particular, ruthenium catalysts have attracted considerable attention because of the widest range of accessible oxidation states, coupled with some unique mechanistic and selectivity features.[9]

Dioxygenase activity has been demonstrated for ruthenium porphyrins, capable of aerobic epoxidation in organic solvents under mild temperature and pressure conditions.[10,11] In this system, a $Ru^{II}/Ru^{IV}/Ru^{VI}$ manifold operates under turnover conditions, whereby the competent oxidant, a *trans*-dioxoruthenium(VI) porphyrinato complex, is formed by disproportionation of a $Ru^{IV}$=O precursor, generated from the reduced $Ru^{II}$ state under oxygen atmosphere. The mechanistic features of the ruthenium-based dioxygenase catalysis are of outmost importance, as they overcome the need of a sacrificial co-reductant, usually employed for restoring the catalyst in its lowest oxidation state, to interact with oxygen. However the scarce resistance of porphyrins towards oxidative degradation limits its efficiency to ca. 50 turnovers (TON), and yields generally slow turnover frequency (TOF) of 1–2 turnovers per hour.

In this light, the use of a totally inorganic ligand system derived from molecular polyoxometalates (POMs), is emerging as a rewarding strategy to the design of innovative catalysts with improved stability for recycling aims.[12–19] Indeed, POMs provide a wide range of structures and coordination geometries to include one or more multi-redox active transition metal centers, enabling catalysis.[12–19] The polyanionic nature of POM ligands offers a straightforward tool for solubility tuning, encompassing a large variety of media, from aqueous to organic or perfluorinated phases,[20–22] including also ionic liquids.[23–27]

[a] Dr. A. Sartorel, Dr. M. Carraro, Dr. S. Berardi, Prof. A. Bagno, Prof. M. Bonchio
ITM-CNR and Department of Chemical Sciences
University of Padova Via F. Marzolo, 1, 35131 Padova (Italy)
E-mail: marcella.bonchio@unipd.it

[b] Dr. P. Miró, Dr. C. Bo
Institute of Chemical Research of Catalonia (ICIQ)
Av. Països Catalans 16, 43007 Tarragona (Spain)
E-mail: cbo@iciq.es

[c] Prof. O. Bortolini
Department of Chemical and Pharmaceutical Sciences
University of Ferrara
via Fossato di Mortara 17-19, 44121 Ferrara (Italy)

[d] Dr. C. Bo
Departament de Química Física i Inorgànica
Universitat Rovira i Virgili c/Marcel·lí Domingo s/n
Campus Sescelades, 43007 Tarragona (Spain)

Supporting information for this article is available on the WWW under http://dx.doi.org/10.1002/chem.201404088.

Moreover the electron-withdrawing character of the metal-oxide framework is predicted to enhance the reactivity of high-valent transition-metal intermediates and assist deprotonation equilibria taking place on the polyoxygenated surface.[28,29] As an example, iron-substituted POMs, with 2 to 6 iron centers, have shown intriguing structural and reactivity features that are reminiscent of bioinspired oxygenase models.[30] With the same aim, the synthesis of ruthenium analogues is posing a major synthetic challenge, owing to its inertness with respect to ligand exchange, the mixed-valence nature of generally used precursors, and the need for extensive purification steps. These arguments apply to the original report by Neumann et al., on the dioxygenase activity by the $[(WZnRu^{III}_2(OH)(H_2O))(ZnW_9O_{34})_2]^{11-}$ sandwich-type ruthenium polyoxotungstate, originally claimed to perform adamantane hydroxylation with unmatched selectivity under aerobic conditions and in organic media,[31,32] although the actual nature of the species and the selectivity in the oxidation process have been subsequently questioned and revised by Finke et al.[33,34] These studies have stimulated a great deal of research activity focusing on the design of novel ruthenium-substituted POMs, with special emphasis to water soluble systems. The formidable challenge is indeed the stabilization of high-valent ruthenium-peroxo or oxene intermediates following bioinspired guidelines, but carving new pathways within the totally inorganic POM environment. Such breakthrough perspective has been recently achieved for water oxidation enabled by ruthenium-based POMs in aqueous media and under very mild conditions thus mimicking the natural oxygen-evolving center of the photosynthetic II enzyme.[12–19,35–37]

We present herein, a combined experimental and computational study on the synthesis, characterization, catalytic activity and oxygenase mechanism of the single-site ruthenium catalysts with general formula $\alpha$-$[Ru^{II/III}(DMSO)XW_{11}O_{39}]^{n-}$ (X = P, Si; $n$ = 4–6 depending on the heteroatom X and on Ru oxidation state; DMSO = dimethylsulfoxide), hereafter indicated as Ru(DMSO)$XW_{11}$. These isostructural complexes feature a hybrid ligand system with one apical DMSO molecule and a pentaoxygenated binding site provided by the $\alpha$-Keggin polyoxotungstate residue where four coordination positions lie on the equatorial plane. Owing to the striking analogy of its coordination geometry, the mono-lacunary polyoxotungstate ligand has been described as the inorganic mimicry of natural heme-ligands (Scheme 1).[38–42] Our experimental approach exploits the strong acceleration induced upon microwave (MW) irradiation of polyelectrolyte water solutions, thus applying to both POM metalation with ruthenium precursors[43] and the screening of oxygenation catalysis by the resulting ruthenium-substituted species.

The paper addresses several aspects: (i) optimized MW-assisted synthesis (especially in comparison to hydrothermal procedures)[44,45] and purification protocol of monoruthenium-substituted POMs, (ii) their solution characterization by converging spectroscopic techniques, including elemental analysis, infrared spectroscopy, ESI-MS spectrometry, cyclic voltammetry, heteronuclear NMR ($^{29}$Si, $^{31}$P and $^{183}$W), EPR, and magnetic-moment determinations, (iii) dissection of a $Ru^{III}/Ru^{V}$ manifold for catalytic aerobic oxidation in water under MW irradiation. In particular DFT calculations envisage a low-energy pathway involving the participation of a Ru(IV)-$\mu$-peroxo dimer evolving to an active Ru(V)-oxo species as postulated for the organic porphyrin analogues.[9–11]

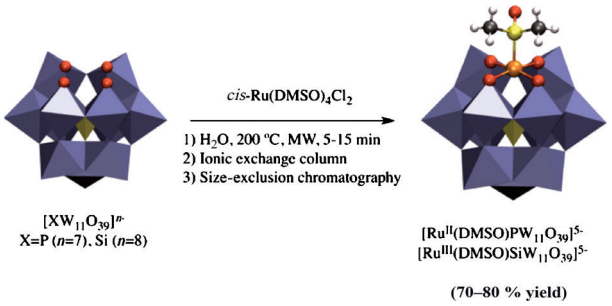


**Scheme 1.** MW-assisted hydrothermal metalation of lacunary $\alpha$-Keggin species. Color code: $WO_6$ octahedra iceblue, $XO_4$ tetrahedra yellow, Ru orange, O red, S yellow, C grey and H white.

## Results and Discussion

### MW-assisted synthesis and purification of $\alpha$-$[Ru^{II/III}(DMSO)XW_{11}O_{39}]^{n-}$ (X = P, Si; $n$ = 4–6)

Lacunary POMs with missing metallic addenda are key intermediates for the incorporation of hetero transition-metal cations. In particular, mono-lacunary $\alpha$-Keggin anions with general formula $[XW_{11}O_{39}]^{n-}$ (X = B, Si, Ge, P, As), represent a unique class of ligands. They provide a planar tetradentate binding site with a proximal axial coordination position, and as such, they have been considered the inorganic porphyrin analogue.[38–42] POM metalation with ruthenium is not straightforward, and high temperatures and prolonged reaction times are generally needed.[44,45] Ruthenium precursors such as $RuCl_3{\cdot}nH_2O$, $[Ru(H_2O)_6][C_7H_7SO_3]_2$, $Ru(acac)_3$ (acac = acetylacetonate), $K_4[Ru_2OCl_{10}]$ and *cis*-$RuCl_2(DMSO)_4$ have been used under different experimental conditions.[46–60] In the most recent and efficient synthetic protocols, the reagent of choice has been *cis*-$RuCl_2(DMSO)_4$. We have previously reported that fast and selective metalation of $\alpha$-$[PW_{11}O_{39}]^{7-}$ with $RuCl_2(DMSO)_4$ can be achieved in water, under microwave (MW) irradiation.[43] The MW-assisted hydrothermal process leads to the highly selective incorporation of a ruthenium atom into the POM framework in 5 to 15 min (Scheme 1). The diamagnetic, air-stable, $Li_5[Ru^{II}(DMSO)PW_{11}O_{39}]$ complex can be isolated, after purification on ion-exchange and size exclusion columns, in 70–80% yields on a gram scale. The progress and the selectivity of the POM metalation can be monitored by $^{183}$W NMR as the free ligand and the tungstoruthenate complex give rise to two distinct sets of six resonances.

The same protocol has been also applied to the metalation of the isostructural $\alpha$-$[SiW_{11}O_{39}]^{8-}$ ligand. After cation exchange and purification by exclusion dimensional chromatography, the paramagnetic complex $Li_5[Ru^{III}(DMSO)SiW_{11}O_{39}]$ is obtained in 70% yield. The efficiency of microwave flash heating in acceler-

ating chemical transformations is well recognized, reducing reaction times from days and hours to minutes and seconds. Of particular interest is therefore the application of new MW-assisted methodologies to inorganic synthesis and fast catalysis. In this respect, the use of robust polyanionic catalysts, especially in water as solvent, represents a specific advantage considering that polar and ionic conducting media lead to an extremely rapid MW-induced in situ heating. This is expected to produce an efficient thermal activation under controlled and safer conditions. The application of MW-induced dielectric heating under turnover conditions will be further addressed in the following paragraphs.

### Characterization of α-$[Ru^{II/III}(DMSO)XW_{11}O_{39}]^{n-}$ (X = P, Si, n = 4–6).

#### *Infrared spectroscopy*

Analysis of the FT-IR spectra gives a straightforward tool to ascertain POM metalation. In fact the incorporation of ruthenium in the POM vacancy partially restores the symmetry of the saturated Keggin structure, leading to a decrease in the number of IR absorptions and to an increase in their frequency, as it results from a direct comparison of the mono-lacunary α-Keggin anions $[PW_{11}O_{39}]^{7-}$ and $[SiW_{11}O_{39}]^{8-}$ spectra with those of $[Ru^{II}(DMSO)PW_{11}O_{39}]^{5-}$ and $[Ru^{III}(DMSO)SiW_{11}O_{39}]^{5-}$ (Figure S1 in the Supporting Information). For $[Ru^{II}(DMSO)PW_{11}O_{39}]^{5-}$ and $[Ru^{III}(DMSO)SiW_{11}O_{39}]^{5-}$, the absorptions at ca. 930–980 $cm^{-1}$ are attributed to the terminal W=O, while the one at ca. 750–780 $cm^{-1}$ is attributed to the corner-sharing and edge-sharing octahedra W-O-W. A computational analysis has been used to validate these spectral assignments (Table S1 in the Supporting Information for details). The FT-IR analysis is therefore consistent with the α-Keggin structure of the ruthenium complexes.

#### *Electrospray ionization mass spectrometry*

The relevance of electrospray ionization mass spectrometry (ESI-MS) for both the characterization of isolated POMs, and for the design of novel polyoxometalate architectures has been recently demonstrated.[61,62] The *m/z* value and the isotopic signature pertaining to the multimetal polyanionic cluster provide direct evidence of the POM solution speciation (Figure 1). For $Li_5[Ru^{II}(DMSO)PW_{11}O_{39}]$, two signals are observed at *m/z* 954 and 1438, attributed to $Li_2[Ru(DMSO)PW_{11}O_{39}]^{3-}$ and $Li_3[Ru(DMSO)PW_{11}O_{39}]^{2-}$. The calculated isotopic envelope for the triply-charged ion at *m/z* 954 (*m/z* spacing of 0.33 units) is also in good agreement with the proposed assignment. The corresponding peaks for $Li_5[Ru^{III}(DMSO)SiW_{11}O_{39}]$ are found at *m/z* 953 and 1435, and attributed respectively to the triply- and doubly-charged anion $HLi[Ru(DMSO)SiW_{11}O_{39}]^{3-}$ and $HLi_2[Ru(DMSO)SiW_{11}O_{39}]^{2-}$.

#### *Cyclic voltammetry (CV)*

Inspection of the CV curves for the isolated complexes $[Ru^{II}(DMSO)PW_{11}O_{39}]^{5-}$ and $[Ru^{III}(DMSO)SiW_{11}O_{39}]^{5-}$ indicates that the redox potentials relative to the $Ru^{III}/Ru^{II}$ reversible waves

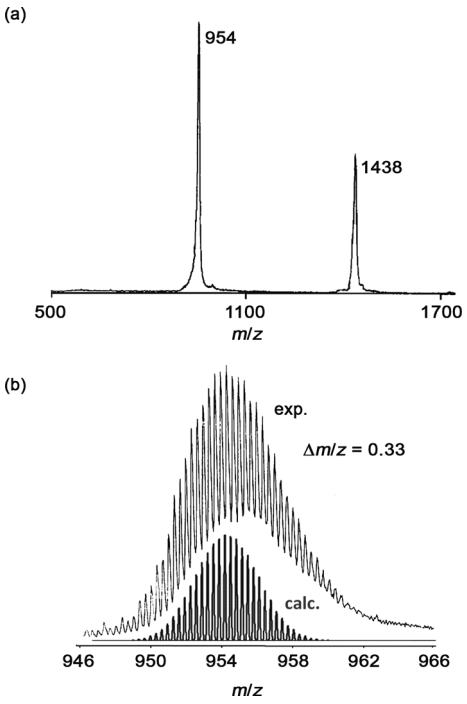


**Figure 1.** ESI-MS spectrum of $Li_5[Ru^{II}(DMSO)PW_{11}O_{39}]$; experimental and calculated isotopic envelope obtained for the triply-charged anion attributed to $Li_2[Ru(DMSO)PW_{11}O_{39}]^{3-}$.

differ by ca. 200 mV, being $E_{1/2} = 379$ mV (peak separation $\Delta E_p = 60$ mV) for $[Ru^{III/II}(DMSO)PW_{11}O_{39}]^{4/5-}$ and $E_{1/2} = 186$ mV for $[Ru^{III/II}(DMSO)SiW_{11}O_{39}]^{5/6-}$ ($\Delta E_p = 60$ mV) versus Ag/AgCl in 3 M NaCl (Figure 2). This feature can be associated to the higher negative charge of the undecatungstosilicate ligand with respect to the tungstophosphate analogue, favoring the one-electron oxidation of the $Ru^{II}$ and its evolution to the $Ru^{III}$ species under the adopted synthetic conditions. One-electron waves with $E_{1/2} = 1390$ mV ($\Delta E_p = 70$ mV) and $E_{1/2} = 1185$ mV ($\Delta E_p = 60$ mV) are then observed for the phosphotungstate and silicotungstate derivatives respectively, which have been found independent of the pH conditions, varied in the range 3–6. As recently reported, this observation is consistent with a $Ru^{IV}/Ru^{III}$ redox couple, whereby DMSO is still bound to the ruthenium center.[60] Noticeably, the corresponding aquo com-

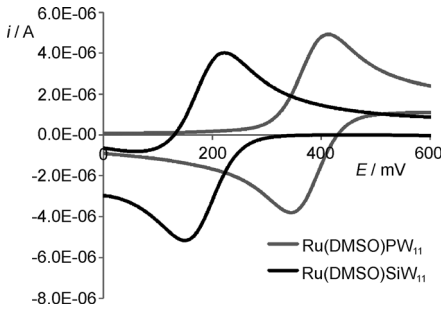


**Figure 2.** Zoom in cyclic voltammograms of 1 mM $Ru^{II}(DMSO)PW_{11}$ and $Ru^{III}(DMSO)SiW_{11}$ in $KH_2PO_4$ 0.5 M (pH 4.23). Working electrode: glassy carbon, counter electrode: Pt; reference electrode: Ag/AgCl (3 M NaCl); scan rate 100 mV $s^{-1}$.

plex $Ru^{III}(H_2O)XW_{11}$, (X = Si, P) gives rise to a bi-electronic wave, ascribed to the formation of a $Ru^{V}$–oxo species.[63] This latter has been proposed as the competent oxygen transfer agent under electrocatalytic conditions.

### *Heteronuclear NMR studies*

NMR characterization of $Li_5[Ru^{II}(DMSO)PW_{11}O_{39}]$ ($^1H$, $^{31}P$, $^{183}W$) was reported by the group of Pope[63] and was confirmed by our data, including also the registration of $^{99}Ru$ NMR spectra, where a signal at $\delta = 7737$ ppm is observed, which was the first example of $^{99}Ru$ NMR for ruthenium embedded in a POM matrix.[43] $^1H$ and $^{31}P$ NMR show the expected singlet resonances at 3.4 and 10.8 ppm, respectively; the former is attributed to the protons of the methyl groups of the S-bound DMSO ligand, as has been recently proved by crystallographic analysis.[51] $^{183}W$ NMR shows the 6 resonances at 117.4, −2.7, −94.4, −105.8, −133.3, and −145.1 ppm with relative intensity 2:2:2:1:2:2. The paramagnetic nature of the analogous $Ru^{III}$ complex $Li_5[Ru^{III}(DMSO)SiW_{11}O_{39}]$, render the NMR characterization less informative. The $^1H$ NMR signal of the methyl protons of the bound DMSO is not observed, while the $^{29}Si$ NMR exhibits a broad signal at $\delta = -92$ ppm ($W_{1/2} = 150$ Hz) insensitive to pH in the range 3–8. Finally, $^{183}W$ NMR shows 5 broad signals with relative intensity 2:4:2:2:1 between −120 and −250 ppm (Figure 3a); the very broad signal at −145 ppm is probably due to the collapsing of the resonances of two nonequivalent tungsten sites. Noteworthy, a most informative NMR characterization of this species is achieved by in situ reduction of $Ru^{III}$ to $Ru^{II}$ with one equivalent of ascorbic acid, forming the diamagnetic $[Ru^{II}(DMSO)SiW_{11}O_{39}]^{6-}$. A well resolved $^{183}W$ NMR system is thus registered, with six sharp signals of relative intensity 2:2:2:1:2:2 (Figure 3b), as expected from the $C_s$ symmetry of the species. Once again, the presence of two strongly deshielded signals at 111.6 and −15.5 ppm is in agreement with the incorporation of ruthenium in the POM vacancy. As expected, a sharp signal at $\delta = -81.3$ is obtained also for the $^{29}Si$ NMR spectrum (see Figure S2 in Supporting Information), while in $^1H$ NMR the resonance of the methyl protons of bound DMSO is observed at $\delta = 3.34$.

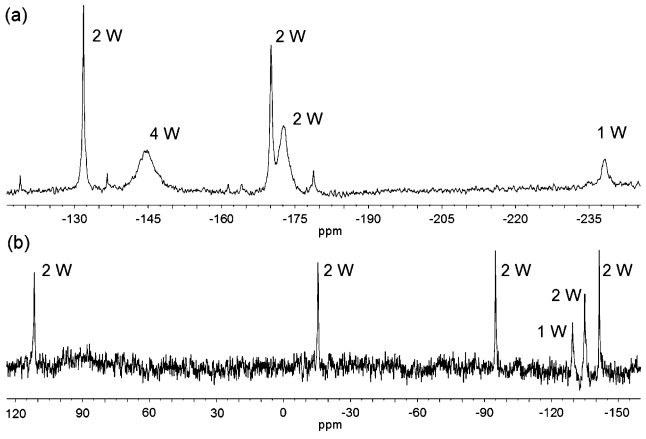


**Figure 3.** (a) $^{183}W$ NMR spectra of $[Ru^{III}(DMSO)SiW_{11}O_{39}]^{5-}$ and (b) $^{183}W$ NMR spectra of $[Ru^{II}(DMSO)SiW_{11}O_{39}]^{6-}$ produced in situ.

### *Solution magnetic-moment determination and EPR spectrum*

The paramagnetism of $[Ru^{III}(DMSO)SiW_{11}O_{39}]^{5-}$ species was confirmed by measurement of its magnetic moment in solution with Evans' method.[64] The resulting value of 1.9 μB is in agreement with a low-spin paramagnetic $Ru^{III}$ center within an octahedral coordination environment, yielding values in the range 1.8–2.0 μB;[65–68] convergent evidence is provided by EPR analysis of the tetra-*n*-butylammonium salt of $[Ru^{III}(DMSO)SiW_{11}O_{39}]^{5-}$ in frozen acetonitrile, where three major lines at *g* values of 2.29, 2.19 and 1.88 are observed, characteristic of a rhombic system and in agreement with literature data.[69–77] This is also consistent with the calculated electronic structure for such compound, that predicts a ground state doublet (see below).

## Aerobic oxidation in water: catalytic oxygenation of DMSO by α-$[Ru^{II/III}(DMSO)XW_{11}O_{39}]^{n-}$

Electrocatalytic oxidation of DMSO catalyzed by $[Ru^{III}(H_2O)PW_{11}O_{39}]^{4-}$ was reported by Pope et al. who indicated a high-valent $Ru^{V}{=}O$ intermediate as the competent species for catalytic oxygen transfer.[63] Herein, oxygen transfer to DMSO has been chosen as the model reaction to probe the POM effect and its evolution under aerobic conditions in water.[78] The reaction is performed under oxygen atmosphere ($PO_2 = 1$ atm), buffer solution (pH 4.8) and MW-irradiation, leading to dimethylsulfone ($DMSO_2$). The selective production of the sulfone rules out the major incursion of radical pathways.[78] Control experiments in the absence of the ruthenium species or in the presence of the Ru-free POM ligand confirm that no oxidation of DMSO is observed. The kinetic profile of the oxidation, is conveniently monitored by $^1H$ NMR and shows a zero-order behavior in DMSO, for both $Ru^{II}(DMSO)PW_{11}$ and $Ru^{III}(DMSO)SiW_{11}$ catalysts (Figure 4a).

The rate of substrate conversion depends on the nature of the POM ligand, whereby $Ru^{II}(DMSO)PW_{11}$ is more reactive than $Ru^{III}(DMSO)SiW_{11}$, with turnover frequency of 2.0 versus 1.3 TON per hour, respectively. Moreover, the oxidation rate depends also on the POM counter cation. Indeed, the reaction catalyzed by $Ru^{II}(DMSO)PW_{11}$ and performed in acetate buffers, HOAc/MOAc pH 4.8, with different alkaline salts ($M = Li^+$, $Na^+$, $K^+$), yields the kinetic profiles reported in Figure 4b. The reactivity increases in the order $K^+ < Li^+ < Na^+$, with observed turnover frequency of 1.1, 2.0, and 2.9 TON $h^{-1}$ respectively (in the presence of $K^+$ ions, the rate of the reaction also slows down after ca. 120 min). The influence of the counter cation on the redox properties of POM anions has been documented in the recent literature, ascribed to formation of ion pairs,[79–82] which might lead to a modification of the effective charge of the POMs, thus affecting their solvation and modifying their catalytic behavior.[35,83–85] Furthermore, a secondary effect is expected because of the different conductivity of the three alkali cations in aqueous solution.[86] This induces a differential MW

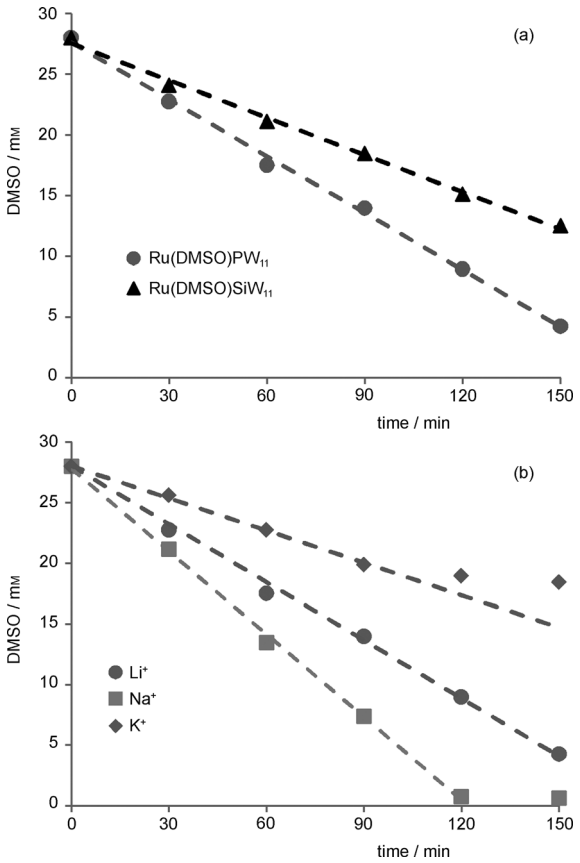


**Figure 4.** (a) Oxidation of DMSO (28 mM) catalyzed by $Ru^{III}(DMSO)SiW_{11}$ and $Ru^{II}(DMSO)PW_{11}$ (4.7 mM) in 0.1 M lithium acetate buffer (pH 4.8), $PO_2 = 1$ atm; (b) oxidation of dimethylsulfoxide catalyzed by $Ru^{II}(DMSO)PW_{11}$; conditions: 0.1 M lithium, sodium or potassium acetate buffer (pH 4.8), $PO_2 = 1$ atm. In all the reactions microwave induced dielectric heating was applied (300 W for 3 min and 150 W for 30 min; $T_{bulk} = 200\,^{\circ}C$).

absorption, and a consequent difference for the heating profiles and distribution of the so-called overheated zones (hot spots) of the solvent, which also affect the oxidation rate. Therefore the resulting oxidation rates are likely to depend from a complex balance of different causes.

### *Catalyst resting state under turnover conditions*

The identity/stability of the $Ru^{II}(DMSO)PW_{11}$ catalyst, has been investigated under turnover conditions directly in situ or upon precipitation as the insoluble $Cs^+$ salt from the reaction mixture. After cation exchange and recovery of the lithium salt, analysis of the FT-IR spectra reveals that the catalyst maintains the pristine structure, with the ruthenium center being still incorporated within the polyoxometalate framework. However, the isolated complex is paramagnetic with a magnetic moment of 1.8 μB, indicative of a $Ru^{III}$ derivative. Accordingly, the $^{31}P$ NMR spectra shows a broad signal at $\delta = -37$ ($W_{1/2} =$ 300 Hz) insensitive to pH in the range 2–9 (Figure S3 in the Supporting Information). This observation rules out the presence of a water molecule as terminal ligand of the ruthenium(III) center, since an acid–base equilibrium would be expected for the aquo complex, producing a variation of the $^{31}P$ NMR chemical shift with the solution pH.[63] This was confirmed by the independent synthesis of $[Ru^{III}(H_2O)PW_{11}O_{39}]^{4-}$ by metalation of $K_7[PW_{11}O_{39}]$ with $Ru(acac)_3$ at high temperature with MW-induced dielectric heating ($T_{bulk} = 200\,^{\circ}C$). Fitting of the $^{31}P$ NMR chemical shift variation at different pH values, gives a $pK_a$ value of 4.9, in good agreement with the literature determination of 5.1 (Figure S4 in the Supporting Information). The ESI-MS results of $Ru(DMSO)PW_{11}$ under turnover conditions are also in agreement with this conclusion, yielding two cluster distributions centered at 952 and 1434, attributed to $H[Ru^{III}(DMSO)PW_{11}O_{39}]^{3-}$ and $Li_2[Ru^{III}(DMSO)PW_{11}O_{39}]^{2-}$, respectively, suggesting the residual presence of dimethylsulfoxide as the apical ligand of ruthenium. Indeed, addition of 1 equivalent of a reducing agent such as ascorbic acid to the recovered catalyst leads to reduction of $Ru^{III}$ to $Ru^{II}$, restoring the catalyst in its initial state, $Ru^{II}(DMSO)PW_{11}$, as confirmed by the appearance of the sharp signal in the $^{31}P$ NMR signal ($\delta = -10.8$ ppm, $W_{1/2} = 300$ Hz) and of the $^1H$ NMR resonance at 3.4 ppm owing to the methyl protons of the DMSO molecule bound to $Ru^{II}$. Therefore, convergent evidence indicate that, under turnover conditions, the catalyst resting state is the paramagnetic complex $[Ru^{III}(DMSO)PW_{11}O_{39}]^{4-}$. Worthy of notice is that the $Ru^{III}$ state, isolated after aerobic oxidation, is readily accessed in situ in the same media by oxidation of the $Ru^{II}$ initial complex with stoichiometric addition of the so called "shunt oxidants" like periodate or oxone. For the parent silicotungstate derivative, the recovered form of the catalyst displays identical structural features as its initial state, thus confirming the residual presence of the $Ru^{III}(DMSO)$ moiety coordinated by the POM framework. Given this common aspect of both catalytic manifolds, the comparison of their performance is straightforward, with the observed difference ascribable to a role of the POM ligand.

### Mechanism of catalytic aerobic oxidation of DMSO

The zero-order kinetics, as it results from the plots of substrate conversion versus time in Figure 4, are indicative of a rate-determining step occurring before oxygen transfer to DMSO. To gain more insights into the catalyst evolution along the reaction coordinate, the dependence of the oxidation rate on its concentration has been analysed. Inspection of graphs in Figure 5, and in particular the second order polynomial fitting of rate versus catalyst concentration (Figure 5a), together with the $1.70 \pm 0.12$ slope from the log/log fitting (Figure 5b), suggests a second order dependence on the catalyst concentration, thus implying that: (i) POM transformation is involved in the rate-determining step, and (ii) this occurs by a bimolecular event. On the other hand, DMSO oxidation performed under pure oxygen atmosphere occurs 7 times faster than under air. On these basis, we propose a catalytic cycle for dioxygen activation by the POM catalyst (Figure 6) displaying some fundamental analogies to ruthenium porphyrin chemistry.[10,11] In agreement with the zero-order kinetics in [DMSO], $[Ru^{III}(DMSO)XW_{11}O_{39}]^{n-}$ acts as an off-cycle catalyst reservoir at low temperature,[87] entering the mechanistic scene by ligand exchange and formation of the aquo complex in water medium (see below) that become predominant at high temperatures

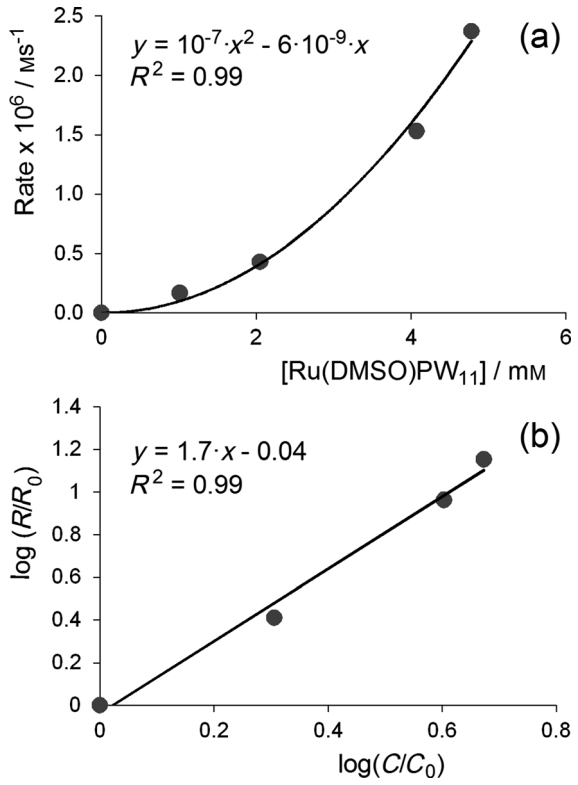


**Figure 5.** (a) Rate of DMSO oxidation versus $Ru^{II}(DMSO)PW_{11}O_{39}$ concentration and (b) plot of $\log(R/R_0)$ versus $\log(C/C_0)$, where $R$ = rates and $C$ = catalyst concentration; the fitted slope results $1.70 \pm 0.12$, indicating possible deactivation pathways occurring for the catalyst package at higher concentration (see text).

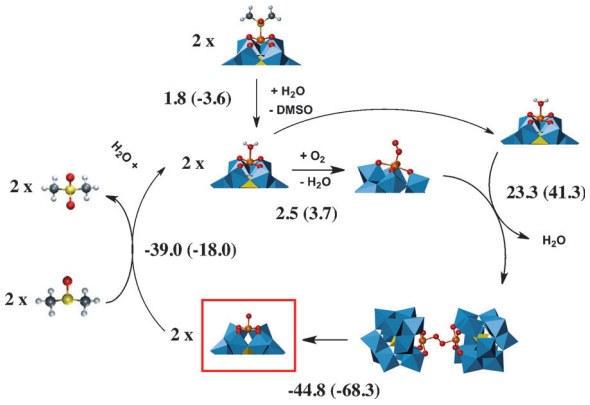


**Figure 6.** Mechanism of DMSO aerobic oxidation catalyzed by $Ru^{III}$-$(DMSO)SiW_{11}$, with $\Delta G$ of the step expressed in kcal mol$^{-1}$ at room temperature and at 250 °C (in parenthesis). The proposed catalytically active species is highlighted in a red square.

(Figure 7). Dioxygen activation can thus be envisaged through reaction of $O_2$ with the $Ru^{III}$ center forming a ruthenium(IV) super-oxo species, than evolving to a dimeric μ-peroxo $Ru^{IV}$-(OO)-$Ru^{IV}$ intermediate by a bimolecular step with a second molecule of the Ru aquo complex. Homolytic cleavage of the μ-peroxo bond leads to a high-valent $Ru^{V}$=O species, being the

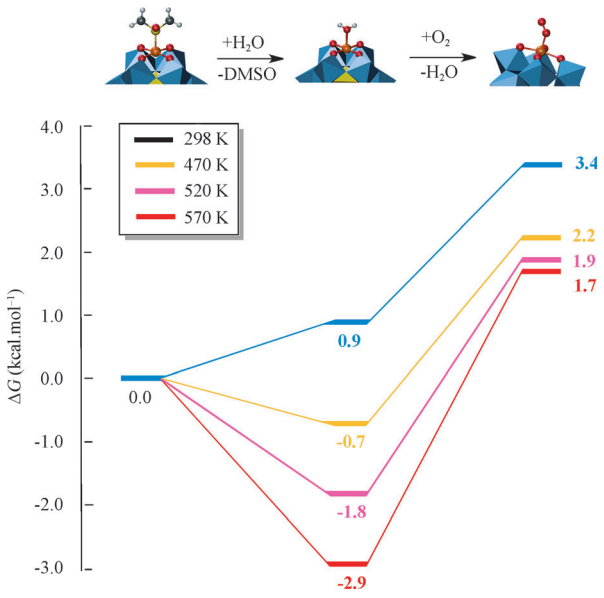


**Figure 7.** Ligand-exchange energetics for $Ru^{III}(L)SiW_{11}$ (L = DMSO, $H_2O$ and $O_2$); $\Delta G$ of the steps expressed in kcal mol$^{-1}$ at different temperatures.

active oxidant, capable of oxygen transfer to DMSO,[63] finally restoring the $Ru^{III}$ state of the catalytic manifold.

This mechanistic scenario is consistent with an overall second-order dependence of the oxidation rate on the catalyst concentration, as the rate-determining step can result from bimolecular steps, that is, the formation of the dimeric peroxo derivative or its evolution to the $Ru^{V}$=O species. Similar intermediates have been proposed for both $Ru^{II}$ or $Ru^{III}$ precursors.[88–90] This mechanistic hypothesis has been addressed by density functional theory calculations using a well-established procedure.[91–93] All the species involved in the catalytic routine have been geometrically optimized and different spin states have been considered. Only the most stable and/or relevant structures are discussed in the text, furthermore all the details have been included in the Supporting Information. Given the experimental observation that the resting state of the catalyst is $Ru^{III}(DMSO)XW_{11}$, (X = Si, P) initial efforts have been dedicated to characterize these species computationally. As expected, the most stable electronic state of $Ru^{III}(DMSO)XW_{11}$ is a low-spin doublet ($S = {}^1/_2$). DMSO is still S bound to $Ru^{III}$, with a S–Ru distance of 2.26 Å, close to the experimental value of 2.19 Å obtained from X-ray analysis for $Ru^{III}(DMSO)SiW_{11}$.[51]

The MW-induced heating ($T_{bulk}$ = 200 °C) and higher temperature hot spots provide the energy required to allow ligand substitution at the $Ru^{III}$ center, with removal of DMSO and coordination of water. This process is thermodynamically disfavored by 0.9 kcal mol$^{-1}$ at room temperature but becomes favorable at high temperature (Figure 7). Therefore only results for $Ru^{III}(DMSO)SiW_{11}$ at $T$ = 250 °C are presented here (250 °C were considered to account of MW-induced hot spots, see the Supporting Information for other temperatures and species). The catalytic cycle starts with ligand exchange at the ruthenium center of the paramagnetic $Ru^{III}(H_2O)SiW_{11}$ (doublet as the most stable spin state). The water ligand exchange by molecu-

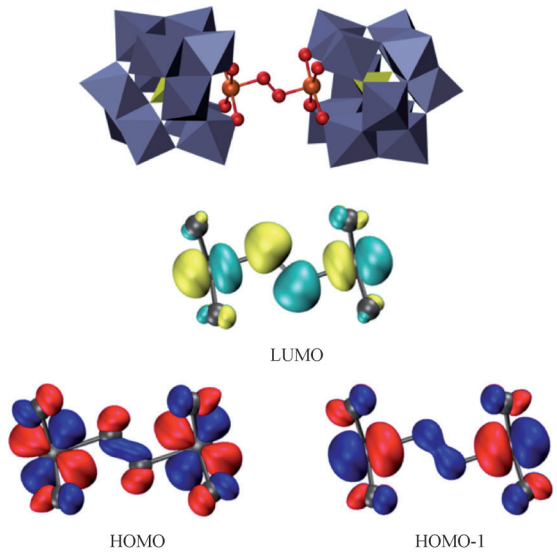


**Figure 8.** Structure for $[(\mu\text{-}O_2)(Ru^{IV}SiW_{11}O_{39})_2]^{10-}$ species (top) and a detailed view of the HOMO-1 to LUMO molecular orbitals in the Ru-$O_2$-Ru moiety (bottom).

lar oxygen is slightly disfavored by 3.7 kcal mol$^{-1}$. End-on coordination of $O_2$ to $Ru^{III}$ leads to the formation of $Ru^{IV}(\eta^1\text{-}O_2)XW_{11}$ (doublet) super-oxide. This coordination is always favored with respect to any of the possible side-on coordination modes that will involve a heptacoordinated ruthenium center. Coordination of $O_2$ is accompanied by oxidation of the $Ru^{III}$ to $Ru^{IV}$ by an internal electron transfer to the $\pi^*$ orbitals of the $O_2$ ligand, weakening the O–O bond and increasing its length by ca. 0.07 Å. This species reacts then with a second catalyst molecule leading to the formation a dimeric $[(\mu\text{-}O_2)(Ru^{IV}XW_{11}O_{39})_2]^{n-}$ (triplet) species (Figure 8 top), this step being endoergonic by 41.3 kcal mol$^{-1}$. The formation of such intermediate could then be the rate-determining step of the overall mechanism, dictating the catalyst kinetic second order as experimentally observed; more so that a considerable activation energy is likely to be involved in the bridging of the two polyanionic units (which could be favored by the formation of ion pairs that shield the POM negative charges). The $[(\mu\text{-}O_2)(Ru^{IV}SiW_{11}O_{39})_2]^{10-}$ species contain two $Ru^{IV}$ centers and formally a bridging $O_2^{2-}$ ligand displaying a weak O–O bond; 8 electrons are distributed in the Ru MO orbitals. The HOMO is localized on the ruthenium centers (d orbitals) with contributions of the p orbitals of $O_2^{2-}$ and POM oxygen atoms. The HOMO-1 still has some p contribution of the oxygen atoms but also a large contribution of the Ru centers (Figure 8 bottom).

The O–O homolytic cleavage is the plausible further step of the mechanism and can be achieved because of the weakness of the O–O bond and to the antibonding nature of the LUMO (Figure 8 bottom). Indeed, the catalytic cycle evolves through the formation of $Ru^{V}$=O species by the homolytic cleavage of $O_2^{2-}$ bridging ligand, that is a highly favored process (−68.3 kcal mol$^{-1}$). The formed $Ru^{V}(O)XW_{11}$ species (quartet) are highly reactive and capable of oxidize DMSO to dimethylsulfone. The oxo moiety is transferred to the substrate in a exergonic reaction (−18.0 kcal mol$^{-1}$) and the catalyst is reformed by a ligand exchange reaction between the dimethylsulfone and a solvent molecule. The formation of $Ru^{V}$–oxo species has been already proposed in the catalytic chemistry of ruthenium monosubstituted polyoxometalates: these intermediates were indeed considered to be the active species in alkene oxidations by periodate catalyzed by $[Ru^{III}(H_2O)SiW_{11}O_{39}]^{5-}$,[94] and in the electrocatalytic oxidation of dimethylsulfoxide catalyzed by $[Ru^{III}(H_2O)PW_{11}O_{39}]^{4-}$.[63] Notably, high-valent $Ru^{V}$–oxo embedded within $XW_{11}O_{39}^{n-}$ ligands were also observed spectroscopically in a recent report dealing with water oxidation catalysis by such species.[36] The involvement of a $Ru^{V}$=O intermediate in the oxygen transfer step, has been probed also by isotopic labelling studies and by electrocatalytic evidence.

### *Isotopic labelling studies*

In order to get insight into the nature of the competent oxidant, formed along the catalytic cycle, aerobic oxidation of dimethylsulfoxide by $Ru^{II}(DMSO)PW_{11}$ was performed in the presence of $H_2{}^{18}O$. Up to 72% incorporation of $^{18}O$ to dimethylsulfone was observed, whereby this was found to increase linearly with the % $^{18}O$ water in the solvent mixture. Control experiments showed that, while DMSO undergoes fully exchange with labelled water, the oxidation product $DMSO_2$ does not. The observed $^{18}O$ incorporation should be thus ascribed to a metal–oxene intermediate, likely involved in water exchange equilibria prior to oxygen transfer to DMSO. This observation is again consistent with a high-valent $Ru^{V}$=O species, responsible for substrate oxygenation.[95–100] While in heme-type complexes oxygen exchange entails an oxo–hydroxo tautomerism,[101] in the present case where *trans* coordination is prevented by the POM ligand, a *cis*-dihydroxo intermediate can be postulated to trigger oxygen exchange within the coordination sphere of the ruthenium site.[99]

### *Electrocatalytic oxidation of DMSO*

Cyclic Voltammetry (CV) experiments have been performed to show the impact of added DMSO on the electrocatalytic current registered at high applied voltage, for $Ru^{II}(DMSO)PW_{11}$ in aqueous solution (Figure 9). Besides the redox wave at $E=$

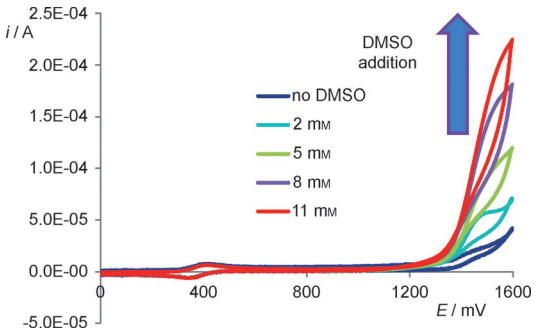


**Figure 9.** Cyclic voltammetry of 1 mM $Ru^{II}(DMSO)PW_{11}$ in the presence of increasing amount of DMSO (2, 5, 8 and 11 mM) in $KH_2PO_4$ 0.5 M (pH 4.23). Working electrode: glassy carbon, counter-electrode: Pt; reference electrode: Ag/AgCl (3 M NaCl), scan rate: 100 mV s$^{-1}$.

379 mV owing to the $Ru^{II} \rightarrow Ru^{III}$ process, the voltammetry of $Ru^{II}(DMSO)PW_{11}$ shows a second oxidation event at 1420 mV, ascribed to a $Ru^{III} \rightarrow Ru^{IV}$ transformation (blue trace in Figure 9).[60,102] When progressive aliquots of dimethylsulfoxide (2–11 mM) are added to the catalyst solution a current increase is observed, owing to catalytic DMSO oxidation.[30]

The catalytic current increases linearly with DMSO concentration in the range 2–11 mM (Figure 9), as expected for a rate-determining chemical step following the electrodic generation of the active catalyst form. Indeed, the electrocatalytic set-up, provides a direct shortcut to the oxygen transfer pathway, described in the mechanistic proposal (left side in Figure 6).

### *Catalyst fate in the spent reaction mixture*

A further piece of information is provided by the analysis of catalyst evolution after prolonged heating in water, but in the absence of DMSO as the substrate. A set of experiments has been designed to analyze possible competing pathways for catalyst transformation which can take the lead, along the oxygenation process, at increasing substrate conversion. Indeed, under the conditions explored (0.1 M lithium acetate buffer pH 4.8, $PO_2 = 1$ atm; MW irradiation $T_{bulk} = 200\,^{\circ}C$), the ruthenium POMs (4.7 mM) undergo a key transformation, as the paramagnetic resting state are lost, to generate diamagnetic derivatives. FT-IR analysis confirms that the ruthenium substituted POM framework is retained, and $^{183}W$ NMR analysis indicates the unequivocal formation of diamagnetic species, exhibiting a spin system different from that of the $Ru^{II}$ precursors. In the case of $Ru^{III}(DMSO)SiW_{11}$, six sharp signals are registered between 10 and −150 ppm with relative intensity 2:2:1:2:2:2 (Figure 10), with one strongly deshielded resonance, as expected from the ruthenium center still embedded in the polyoxotungstate framework. A similar $^{183}W$-NMR behavior is obtained with the tungstophosphate analogue (Figure S5 in the Supporting Information). The aquo complex, $[Ru^{III}(H_2O)SiW_{11}O_{39}]^{5-}$, has been recently shown to evolve to a μ-oxo bridged dimer $[(\mu\text{-}O)(Ru^{IV}SiW_{11}O_{39})_2]^{10-}$ under hydrothermal conditions.[52,103] The dimeric structure of the resulting product, which has been confirmed by crystallographic analysis, accounts for the antiferromagnetic coupling between the metal centers through the μ-oxo bridge, and shows similar NMR features. On this basis, a likely fate of the spent catalytic manifold is the formation of $Ru^{IV}$ μ-oxo dimers.

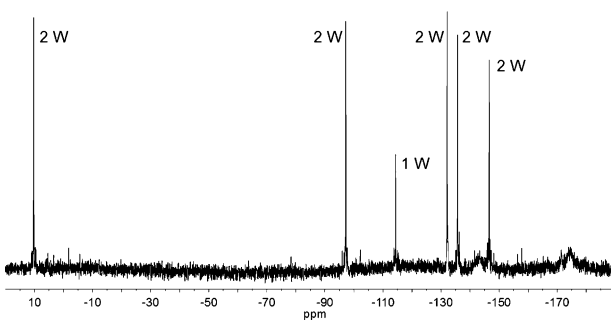


**Figure 10.** $^{183}W$ NMR spectrum of $[(\mu\text{-}O)(Ru^{IV}SiW_{11}O_{39})_2]^{8-}$.

Investigation of the electronic structure of $[(\mu\text{-}O)(Ru^{IV}PW_{11}O_{39})_2]^{8-}$ and $[(\mu\text{-}O)(Ru^{IV}SiW_{11}O_{39})_2]^{10-}$ revealed two formally $Ru^{IV}$ centers connected through a bridging $O^{2-}$ moiety. Both μ-oxo dimers have a singlet ground state with the triplet state lying 6.5 kcal mol$^{-1}$ and 7.4 kcal mol$^{-1}$ higher in energy for the P and Si species respectively, thus confirming their diamagnetic nature. The HOMO and HOMO-1 are localized on the Ru centers and they are combinations of d orbitals, while the LUMO and LUMO + 1 are antibonding combinations of Ru d orbitals and O p orbitals (Figure 11 bottom).

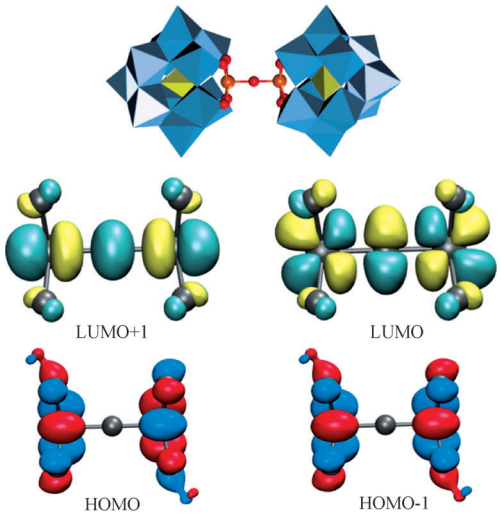


**Figure 11.** Structure of $[(\mu\text{-}O)(Ru^{IV}SiW_{11}O_{39})_2]^{10-}$ (top) an a detailed view of the HOMO-1 to LUMO + 1 molecular orbital in the Ru-O-Ru moiety (bottom). Only the Ru-O-Ru moiety is show for clarity.

The dimerization pathway is disfavoured compared to DMSO oxygenation, however, formation of $[(\mu\text{-}O)(Ru^{IV}XW_{11}O_{39})_2]^{n-}$ dimers can be dominant in the long-term operation. It is worth noting that dimerization through μ-oxo bridges is a well-recognized feature in porphyrin chemistry, being responsible for catalyst deactivation.[104] This observation highlights a further analogy between the transition metal substituted POMs and the bio-inspired mechanisms of metalloporphyrins.

## Conclusion

The emerging properties of ruthenium polyoxometalates as multi-electron catalysts in aqueous environment are herein enhanced under MW-assisted protocols. In particular, MW-induced dielectric heating is confirmed to be an excellent tool to promote the synthesis and reactivity of ruthenium substituted polyoxometalates in water media. In this respect:

1) The MW metalation protocol, initially used for the synthesis of $Li_5[Ru^{II}(DMSO)PW_{11}O_{39}]$, has been successfully extended to the undecatungstosilicate ligand, affording $Li_5[Ru^{III}(DMSO)SiW_{11}O_{39}]$, in 5 min in 70–80% yield and in gram scale.

2) A $Ru^{III}$–$Ru^{V}$ catalytic manifold, stabilized by the POM ligands, is accessed under hydrothermal conditions, enabling dioxygen activation and oxygen transfer in water as probed by the quantitative oxidation of DMSO to sulfone.
3) Kinetic, spectroscopic, and labelling studies, as well as electrocatalytic tests provide converging evidence about the competent role played by the molecular POM species within the turnover routine. The robustness of the inorganic framework and it polyanionic nature are pivotal to sustain and resist the MW heating conditions.
4) DFT studies have been performed to address the proposed mechanistic scenario and the in silico characterization of the key Ru(IV) peroxo dimer, evolving to the high-valent $Ru^{V}$=O species capable of oxygen transfer.
5) The evolution of the catalyst in the spent reaction mixture is taking place by formation of inactive diamagnetic μ-oxo-bridged dimers, isolated and characterized by heteronuclear NMR.

These results delineate a common mechanistic scenario between the ruthenium porphyrin chemistry and its totally inorganic counterpart envisaged with POM ligands. The $Ru^{V}$–oxene generated within the highly electron withdrawing environment of a perfluorinated porphyrin displays some unique reactivity and selectivity features.[96,100] In this perspective the POM alternative offers the unprecedented opportunity to replicate bio-inspired pathways on inorganic molecular metal-oxides, thus bridging the gap with heterogeneous catalysis by active surfaces.[105]

## Experimental Section

### Synthesis of $Li_5[Ru^{II}(DMSO)PW_{11}O_{39}]$

The hydrothermal synthesis of $Li_5[Ru(DMSO)PW_{11}O_{39}]$ was reported in our previous work.[43]

### In situ preparation of $[Ru^{III}(DMSO)PW_{11}O_{39}]^{4-}$

$[Ru^{III}(DMSO)PW_{11}O_{39}]^{4-}$ was prepared in situ by one-electron oxidation of $[Ru^{II}(DMSO)PW_{11}O_{39}]^{5-}$ (4.7 mM) obtained by a stoichiometric addition of $NaIO_4$ or *meta*-chloro-perbenzoic acid. $^{31}P$ NMR: $\delta$ ($H_2O$) = −37 ppm (300 Hz), insensitive to pH in the range 2–9.

### Synthesis of $Li_5[Ru^{III}(DMSO)SiW_{11}O_{39}]$

The synthesis of $Li_5[Ru^{III}(DMSO)SiW_{11}O_{39}]$ was carried in analogous conditions to the undecatungstophosphate derivative. 2.0 g of $K_8SiW_{11}O_{39}{\cdot}13\,H_2O$ (620 mmol) and 0.30 g of $RuCl_2(DMSO)_4$ (620 mmol) were dissolved in 50 mL of $H_2O$ in the closed reactor (HPR-1000/10S, Milestone) and irradiated inside the cavity of the MW Ethos-1600 labstation (Milestone) according to the following parameters: initial power, 350 W; initial time, 2 min; final power, 300 Watt; $T_{bulk}$, 200 °C; reaction time, 5 min. The purification of $Li_5[Ru^{III}(DMSO)SiW_{11}O_{39}]$ can be achieved by chromatography on a Sephadex G-15 column, with water as eluent, isolating the product in 71% yield. IR (KBr): $\tilde{\nu}$ = 1005 (w), 965 (m), 915 (s), 879 (s), 783 (s), 526 (m) $cm^{-1}$; $^{29}Si$ NMR: δ ($D_2O$) = −86 ppm (150 Hz); $^{183}W$ NMR: $\delta$ ($D_2O$) = −131.8 (2W), −144.7 (4W), −170.1 (2W), −172.6 (2W), −238 ppm (1W); MS(ESI): *m/z* (%): 1435 (60), $Li_2H[Ru(DMSO)SiW_{11}O_{39}]^{2-}$; 953 (100), $LiH[Ru(DMSO)SiW_{11}O_{39}]^{3-}$; magnetic moment (Evans' method) $\mu$ = 1.9 $\mu_B$.

### In situ preparation of $[Ru^{II}(DMSO)SiW_{11}O_{39}]^{6-}$

The reduction of $[Ru^{III}(DMSO)SiW_{11}O_{39}]^{5-}$ to $[Ru^{II}(DMSO)SiW_{11}O_{39}]^{6-}$ was achieved directly into an NMR tube by its stoichiometric reaction with ascorbic acid in $D_2O$. $^{183}W$ NMR (0.4 M in $D_2O$): $\delta$ = 111.6 (2W), −15.5 (2W), −94.95 (2W), −129.4 (1W), −134.9 (2W), −141.4 ppm (2W).

### Synthesis of $Li_4[Ru^{III}(H_2O)PW_{11}O_{39}]$

The synthesis of $Li_4[Ru^{III}(H_2O)PW_{11}O_{39}]$ was achieved by stoichiometric reaction of $Ru(acac)_3$ and $K_8SiW_{11}O_{39}$ under dielectric heating induced by microwaves. 2.0 g of $K_8SiW_{11}O_{39}{\cdot}13\,H_2O$ (620 mmol) and 0.247 g of $Ru(acac)_3$ (620 mmol) were dissolved in 50 mL of $H_2O$ in the closed reactor (HPR-1000/10S, Milestone) and irradiated inside the cavity of the MW Ethos-1600 labstation (Milestone) according to the following parameters: initial power, 350 W; initial time, 2 min; final power, 300 W; $T_{bulk}$, 200 °C; reaction time, 30 min. Lithium salt was obtained by cation exchange. The product was purified by exclusion dimensional chromatography. $^{31}P$ NMR, $\delta$ ($D_2O$) = −77 (pH 2.67, $HSO_4^-/SO_4^{2-}$ buffer); −42 (pH 4.09, acetic acid/acetate buffer); 16 (pH 4.59, acetic acid/acetate buffer); 56 (pH 4.85, acetic acid/acetate buffer); 116 (pH 5.24, acetic acid/acetate buffer); 187 (pH 6.12, glutaric acid/glutarate buffer); 218 ppm (pH 7.02, EPPS buffer) .

### Elemental analysis

Elemental analysis were performed by Kanti Labs, Ontario L5T 2G9, Canada. $Li_5[Ru^{II}(DMSO)PW_{11}O_{39}]$: Ru 3.35% (calc. 3.50); W 69.7 (69.95); P 0.85 (1.07); S 1.10 (1.11); C 0.86 (0.83); H 0.23 (0.21); Li 1.25 (1.21). $Li_5[Ru^{III}(DMSO)SiW_{11}O_{39}]$: Ru 3.61% (calc. 3.50); W 70.7 (70.02); Si 0.98 (1.11); C 0.85 (0.83); H 0.24 (0.21); Li 1.31 (1.21).

### Heteronuclear NMR spectroscopy

$^{183}W$ spectra were obtained at 9.4 T (16.67 MHz) on a Bruker Avance DRX 400 instrument, equipped with a standard ($^{31}P$–$^{109}Ag$) 10 mm broadband probe, which could be tuned below its specifications. The $\pi/2$ pulse was ca. 50 μs. $^{183}W$ chemical shifts are externally referenced to 2 M aq $Na_2WO_4$. Typically, ca. $10^3$ transients were collected in 32 K and 1 K data points, respectively. $^{31}P$ and $^{29}Si$ spectra were obtained at 7.0463 T (121.49 and 59.62 MHz respectively) on a Bruker AV 300 instrument, equipped with a multinuclear probe; $^{31}P$ chemical shift are externally referenced to 85% $H_3PO_4$, while $^{29}Si$ chemical shift are externally referenced to a TMS/$CDCl_3$ 1:1 solution.

### ESI-MS characterization

ESI-MS spectra were recorded with a mariner time-of-flight mass Spectrometer (Perspective Biosystem) and with a Finnigan LCQ ion-trap instrument. All experiments were performed in negative mode, through direct infusion by a syringe pump. Standard experimental conditions were as follows: sample concentration: $10^{-3}$ M; mobile phase ($H_2O/CH_3OH$ = 1:1); flow rate: 8 μL $min^{-1}$; nebulizing gas $N_2$: 40 units flow rate; spray voltage: −4.00 kV; capillary voltage: −25 V; capillary temperature: 150 °C; tube lenses offset: 30 V.

### Electrochemistry

Cyclic voltammetry was carried out at room temperature on a BAS Cell Stand C3 electrochemistry workstation (Epsilon). The working electrode was glassy carbon and potentials are given relative to Ag/AgCl reference electrode.

### Magnetic moment

The magnetic moment of ruthenium substituted POM was measured by $^1$H NMR following Evans' methodology, by using acetone or *tert*-butanol as the probe molecules.[64] In a typical experiment, 25 μL of acetone or *tert*-butanol were added to 1 mL of a 30 mM POM solution in $H_2O/D_2O$ 50:50.

### Catalytic aerobic oxidations

The organic substrate was dissolved in 20 mL of 0.1 M acetic acid/acetate buffer (pH 4.8). To this solution catalyst was added, and the solution transferred into a closed reactor (HPR-1000/10S, Milestone) in $O_2$ atmosphere. The microwave heating was performed according to the following parameters: initial power, 300 W (3 min) and 150 W (30 min); $T_{bulk}$, 200 °C. After cooling of the solution, the reactor was opened and a 500 μL aliquot of the solution was taken for monitoring the reaction. Dioxygen atmosphere was restored before performing the successive 30 min cycle of heating. Oxidation of DMSO was monitored by $^1$H NMR, integrating the peaks of DMSO and $DMSO_2$, respectively at $\delta = 2.8$ and 3.4 ppm, referring their area to *tert*-butanol added as external standard. A relaxation delay of 30 s was used to allow full relaxation of the magnetization.

### Isotope labelling studies

Aerobic oxidation of dimethylsulfoxide catalyzed by $Ru(DMSO)PW_{11}$ was carried on in water with 25.6, 17.9 and 13.0% of $H_2{}^{18}O$; the $^{18}O$ content was determined by treating 50 μL of labelled water with 400 μL of a 19.3 mM solution of triethyl orthopropionate in anhydrous $CH_3CN$, followed by GC-MS analysis of the resultant labelled ethyl orthopropionate.[56a] Incorporation of $^{18}O$ in $DMSO_2$ was evaluated by GC-MS after product extraction in $CHCl_3$ (5× volume of water).

### Computational details

All the compounds were geometry optimized with Amsterdam Density Functional (ADF2012).[106,107] These calculations were based on the density functional theory implementation on ADF2012 package using Becke88-Perdew86 exchange correlation functional (BP86).[108–110] The basis set is triple-ζ + polarization Slater-type basis, was used as provided by the ADF library. Zeroth order relativistic approximation (ZORA) was used for the relativistic effects.[111,112] A dielectric cavity was used to account for solvation effects, the conductor-like screening model (COSMO) implemented in ADF.[113] Single-point calculations with M06l functional and the same specifications were performed to evaluate the energy.[114] The calculations took advantage of the highest symmetry available for each species. In the quasiharmonic oscillator approximation, all frequencies below 50 $cm^{-1}$ were replaced by 50 $cm^{-1}$ when computing vibrational free energies, thereby avoiding complications associated with the breakdown of the harmonic oscillator approximation for very-low-frequency normal modes. Some small negative frequencies associated with symmetry breaking and ligand rotations were also replaced by 50 $cm^{-1}$ frequencies. The reaction energies were corrected assuming 1 atm and [Ru species] = 5 mM, $[H_2O] = 55.6$ M and $[DMSO] = [O_2] = [DMSO_2] = 30$ mM.

## Acknowledgements

This work was supported by the Italian MIUR(FIRB "NanoSolar" RBAP11C58Y, PRIN "Hi-Phuture" 2010N3T9M4_001), by Fondazione Cariparo (Nanomode-progetti di eccellenza 2010), by the ICIQ Foundation, Spanish Ministerio de Economia y Competitividad (MINECO, grant CTQ2011-29054-C02-02) and the Generalitat de Catalunya (2009SGR-00259), by the MICINN of the Government of Spain (grants CTQ2008-06549-CO2- 02/BQU, CTQ2004-03346/PPQand CSD2006-0003), and by the CIRIT of the Catalan Government (grants SGR01-00315, 2005SGR00715and 2005SGR00104). P.M. wants to thank the Generalitat de Catalunya for a FI fellowship (2009FIC00026) and the support by University and Research Commission of Innovation, University and Enterprise Department of Catalan Government and European Social Fund. The authors acknowledge the computer resources, technical expertise and assistance provided by the Barcelona Supercomputing Center—Centro Nacional de Supercomputación. COST Action CM1203 "Polyoxometalate Chemistry for Molecular Nanoscience (PoCheMoN)" is gratefully acknowledged.

**Keywords:** catalysis · density functional theory · oxygen activation · polyoxometalate

[1] T. Punniyamurthy, S. Velusamy, J. Iqbal, *Chem. Rev.* **2005**, *105*, 2329–2363.
[2] J. S. Valentine, C. S. Foote, A. Greenberg, J. F. Liebman, *Active Oxygen in Biochemistry*, Springer, Heidelberg, **1995**.
[3] R. Breslow, *Acc. Chem. Res.* **1995**, *28*, 146–153.
[4] B. J. Wallar, J. D. Lipscomb, *Chem. Rev.* **1996**, *96*, 2625–2657.
[5] T. J. Mcmurry, J. T. Groves, *Metalloporphyrin Models for Cytochrome P-450*, Plenum Press, New York, **1986**.
[6] P. C. A. Bruijnincx, G. van Koten, R. J. M. K. Gebbink, *Chem. Soc. Rev.* **2008**, *37*, 2716–2744.
[7] M. Costas, M. P. Mehn, M. P. Jensen, L. Que, *Chem. Rev.* **2004**, *104*, 939–986.
[8] S. S. Stahl, *Angew. Chem.* **2004**, *116*, 3480–3501; *Angew. Chem. Int. Ed.* **2004**, *43*, 3400–3420.
[9] T. Naota, H. Takaya, S. I. Murahashi, *Chem. Rev.* **1998**, *98*, 2599–2660.
[10] J. T. Groves, K. H. Ahn, *Inorg. Chem.* **1987**, *26*, 3831–3833.
[11] J. T. Groves, R. Quinn, *J. Am. Chem. Soc.* **1985**, *107*, 5790–5792.
[12] *Chem. Soc. Rev.* **2012**, *41*, Issue dedicated to Polyoxometalates; Guest Ed.: L. Cronin, A. Müller.
[13] Eur. J. Inorg. Chem. **2013**, Issue dedicated to Polyoxometalates Clusters; Guest Eds.: U. Kortz, T. Liu.
[14] D. L. Long, E. Burkholder, L. Cronin, *Chem. Soc. Rev.* **2007**, *36*, 105–121.
[15] M. T. Pope, *Heteropoly and Isopoly Oxometalates*, Springer, Heidelberg, **1983**.
[16] M. T. Pope, A. Müller, *Polyoxometalate Chemistry: From Topology Via Self-Assembly to Applications*, Kluwer Academic Publishers, Dordrecht, **2001**.
[17] M. Carraro, N. Nsouli, H. Oelrich, A. Sartorel, A. Soraru, S. S. Mal, G. Scorrano, L. Walder, U. Kortz, M. Bonchio, *Chem. Eur. J.* **2011**, *17*, 8371–8378.
[18] A. Sartorel, M. Carraro, G. Scorrano, R. De Zorzi, S. Geremia, N. D. McDaniel, S. Bernhard, M. Bonchio, *J. Am. Chem. Soc.* **2008**, *130*, 5006–5007.

[19] A. Sartorel, P. Miro, E. Salvadori, S. Romain, M. Carraro, G. Scorrano, M. Di Valentin, A. Llobet, C. Bo, M. Bonchio, *J. Am. Chem. Soc.* **2009**, *131*, 16051 – 16053.
[20] M. Carraro, M. Gardan, G. Scorrano, E. Drioli, E. Fontananova, M. Bonchio, *Chem. Commun.* **2006**, 4533 – 4535.
[21] E. de Wolf, G. van Koten, B. J. Deelman, *Chem. Soc. Rev.* **1999**, *28*, 37 – 41.
[22] I. T. Horváth, *Acc. Chem. Res.* **1998**, *31*, 641 – 650.
[23] P. J. Dayson, T. J. Geldbach, *Metal Catalysed Reactions in Ionic Liquids* Springer, Dordrecht, **2005**.
[24] S. Berardi, M. Carraro, M. Iglesias, A. Sartorel, G. Scorrano, M. Albrecht, M. Bonchio, *Chem. Eur. J.* **2010**, *16*, 10662 – 10666.
[25] R. Sheldon, *Chem. Commun.* **2001**, 2399 – 2407.
[26] P. Wasserscheid, W. Keim, *Angew. Chem.* **2000**, *112*, 3926 – 3945; *Angew. Chem. Int. Ed.* **2000**, *39*, 3772 – 3789.
[27] P. Wasserscheid, T. Welton, *Ionic Liquids in Synthesis* Wiley-VCH, Weinheim, **2003**.
[28] A. Sartorel, M. Carraro, A. Bagno, G. Scorrano, M. Bonchio, *Angew. Chem.* **2007**, *119*, 3319 – 3322; *Angew. Chem. Int. Ed.* **2007**, *46*, 3255 – 3258.
[29] K. Sugahara, S. Kuzuya, T. Hirano, K. Kamata, N. Mizuno, *Inorg. Chem.* **2012**, *51*, 7932 – 7939.
[30] A. Sartorel, M. Carraro, G. Scorrano, B. S. Bassil, M. H. Dickman, B. Keita, L. Nadjo, U. Kortz, M. Bonchio, *Chem. Eur. J.* **2009**, *15*, 7854 – 7858.
[31] R. Neumann, M. Dahan, *Nature* **1997**, *388*, 353 – 355.
[32] R. Neumann, M. Dahan, *J. Am. Chem. Soc.* **1998**, *120*, 11969 – 11976.
[33] A. M. Morris, O. P. Anderson, R. G. Finke, *Inorg. Chem.* **2009**, *48*, 4411 – 4420.
[34] C. X. Yin, R. G. Finke, *Inorg. Chem.* **2005**, *44*, 4175 – 4188.
[35] Y. V. Geletii, B. Botar, P. Koegerler, D. A. Hillesheim, D. G. Musaev, C. L. Hill, *Angew. Chem.* **2008**, *120*, 3960 – 3963; *Angew. Chem. Int. Ed.* **2008**, *47*, 3896 – 3899.
[36] M. Murakami, D. C. Hong, T. Suenobu, S. Yamaguchi, T. Ogura, S. Fukuzumi, *J. Am. Chem. Soc.* **2011**, *133*, 11605 – 11613.
[37] M. Sadakane, N. Rinn, S. Moroi, H. Kitatomi, T. Ozeki, M. Kurasawa, M. Itakura, S. Hayakawa, K. Kato, M. Miyamoto, S. Ogo, Y. Ide, T. Sano, *Z. Anorg. Allg. Chem.* **2011**, *637*, 1467 – 1474.
[38] L. C. W. Baker, *Plenary Lecture, XV Int. Conf. on Coord. Chem. Proceedings*, Moscow.
[39] L. C. W. Baker, J. S. Figgis, *J. Am. Chem. Soc.* **1970**, *92*, 3794 – 3797.
[40] C. L. Hill, R. B. Brown, *J. Am. Chem. Soc.* **1986**, *108*, 536 – 538.
[41] D. E. Katsoulis, M. T. Pope, *J. Am. Chem. Soc.* **1984**, *106*, 2737 – 2738.
[42] D. E. Katsoulis, M. T. Pope, *J. Chem. Soc. Dalton Trans.* **1989**, 1483 – 1489.
[43] A. Bagno, M. Bonchio, A. Sartorel, G. Scorrano, *Eur. J. Inorg. Chem.* **2000**, 17 – 20.
[44] M. Higashijima, *Chem. Lett.* **1999**, 1093 – 1094.
[45] S. Ogo, M. Miyamoto, Y. Ide, T. Sano, M. Sadakane, *Dalton Trans.* **2012**, *41*, 9901 – 9907.
[46] J. A. F. Gamelas, H. M. Carapuca, M. S. Balula, D. V. Evtuguin, W. Schlindwein, F. G. Figueiras, V. S. Amaral, A. M. V. Cavaleiro, *Polyhedron* **2010**, *29*, 3066 – 3073.
[47] I. V. Kalinina, N. V. Izarova, U. Kortz, *Inorg. Chem.* **2012**, *51*, 7442 – 7444.
[48] D. Laurencin, R. Thouvenot, K. Boubekeur, P. Gouzerh, A. Proust, *Comptes Rendus Chimie* **2012**, *15*, 135 – 142.
[49] M. Sadakane, M. Higashijima, *Dalton Trans.* **2003**, 659 – 664.
[50] M. Sadakane, S. Moroi, Y. Iimuro, N. Izarova, U. Kortz, S. Hayakawa, K. Kato, S. Ogo, Y. Ide, W. Ueda, T. Sano, *Chem. Asian J.* **2012**, *7*, 1331 – 1339.
[51] M. Sadakane, D. Tsukuma, M. H. Dickman, B. Bassil, U. Kortz, M. Higashijima, W. Ueda, *Dalton Trans.* **2006**, 4271 – 4276.
[52] M. Sadakane, D. Tsukuma, M. H. Dickman, B. S. Bassil, U. Kortz, M. Capron, W. Ueda, *Dalton Trans.* **2007**, 2833 – 2838.
[53] S. W. Chen, R. Villanneau, Y. L. Li, L. M. Chamoreau, K. Boubekeur, R. Thouvenot, P. Gouzerh, A. Proust, *Eur. J. Inorg. Chem.* **2008**, 2137 – 2142.
[54] V. Lahootun, C. Besson, R. Villanneau, F. Villain, L. M. Chamoreau, K. Boubekeur, S. Blanchard, R. Thouvenot, A. Proust, *J. Am. Chem. Soc.* **2007**, *129*, 7127 – 7135.
[55] L. H. Bi, E. V. Chubarova, N. H. Nsouli, M. H. Dickman, U. Kortz, B. Keita, L. Nadjo, *Inorg. Chem.* **2006**, *45*, 8575 – 8583.
[56] Y. Sakai, A. Shinohara, K. Hayashi, K. Nomiya, *Eur. J. Inorg. Chem.* **2006**, 163 – 171.
[57] L. H. Bi, U. Kortz, M. H. Dickman, B. Keita, L. Nadjo, *Inorg. Chem.* **2005**, *44*, 7485 – 7493.
[58] L. H. Bi, F. Hussain, U. Kortz, M. Sadakane, M. H. Dickman, *Chem. Commun.* **2004**, 1420 – 1421.
[59] D. Laurencin, R. Villanneau, H. Gerard, A. Proust, *J. Phys. Chem. A* **2006**, *110*, 6345 – 6355.
[60] S. Ogo, N. Shimizu, T. Ozeki, Y. Kobayashi, Y. Ide, T. Sano, M. Sadakane, *Dalton Trans.* **2013**, *42*, 2540 – 2545.
[61] M. Bonchio, O. Bortolini, V. Conte, A. Sartorel, *Eur. J. Inorg. Chem.* **2003**, 699 – 704.
[62] D. L. Long, C. Streb, Y. F. Song, S. Mitchell, L. Cronin, *J. Am. Chem. Soc.* **2008**, *130*, 1830 – 1832.
[63] C. Y. Rong, M. T. Pope, *J. Am. Chem. Soc.* **1992**, *114*, 2932 – 2938.
[64] I. P. Evans, A. Spencer, G. Wilkinson, *J. Chem. Soc. Dalton Trans.* **1973**, 204 – 209.
[65] F. A. Cotton, R. C. Torralba, *Inorg. Chem.* **1991**, *30*, 4392 – 4393.
[66] L. R. Dinelli, A. A. Batista, K. Wohnrath, M. P. de Araujo, S. L. Queiroz, M. R. Bonfadini, G. Oliva, O. R. Nascimento, P. W. Cyr, K. S. MacFarlane, B. R. James, *Inorg. Chem.* **1999**, *38*, 5341 – 5345.
[67] M. M. Taqui Khan, K. V. Reddy, *J. Coord. Chem.* **1983**, *12*, 71 – 80.
[68] K. Nomiya, H. Torii, K. Nomura, Y. Sato, *J. Chem. Soc. Dalton Trans.* **2001**, 1506 – 1512.
[69] J. Y. Xu, P. Li, X. R. Lin, M. X. Li, S. L. Jin, G. Y. Xie, W. L. Sun, *Chem. J. Chin. Univ. Chin.* **2001**, *22*, 520 – 523.
[70] R. Ben-Daniel, L. Weiner, R. Neumann, *J. Am. Chem. Soc.* **2002**, *124*, 8788 – 8789.
[71] E. Galardon, P. Le Maux, C. Paul, C. Poriel, G. Simonneaux, *J. Organomet. Chem.* **2001**, *629*, 145 – 152.
[72] P. N. Komozin, *Russian J. Inorg. Chem.* **2000**, *45*, 589 – 600.
[73] R. Neumann, A. M. Khenkin, *Inorg. Chem.* **1995**, *34*, 5753 – 5760.
[74] S. Rigaut, O. Maury, D. Touchard, P. H. Dixneuf, *Chem. Commun.* **2001**, 373 – 374.
[75] C. C. Rong, H. So, M. T. Pope, *Eur. J. Inorg. Chem.* **2009**, 5211 – 5214.
[76] P. Sengupta, R. Dinda, S. Ghosh, A. K. Guha, *Trans. Met. Chem.* **2002**, *27*, 290 – 294.
[77] T. D. Thangadurai, K. Natarajan, *Synth. React. Inorg. Met.-Org. Chem.* **2001**, *31*, 549 – 567.
[78] Radical oxidation of aqueous DMSO is expected to yield methanesulfinic acid and other by-products; see R. Herscu-Kluska, A. Masarwa, M. Saphier, H. Cohen, D. Meyerstein, *Chem. Eur. J.* **2008**, *14*, 5880. Under analogous conditions ($PO_2 = 1$ atm, MW irradiation at 300 W for 3 min and 150 W for 30 min; $T_{bulk} = 200\,^{\circ}C$), aerobic oxidation of water soluble phenol, uracil, *cis*-1,2-cyclooctandiol catalyzed by $Li_5[Ru^{II}(DMSO)PW_{11}O_{39}]$ occurs with substrate conversion in the range 70 – 98% after ca. 3 h. Phenol undergoes quantitative conversion, with an overall decrease of the COD content of the aqueous solution up to 30%. With uracil, a $\Delta$COD of 60% is observed at 80% substrate conversion, corresponding to an almost complete degradation of the purinic base. *cis*-1,2-cyclooctandiol is subjected to ring cleavage, yielding octandial and suberic acid as the main products.
[79] K. Heussner, K. Peuntinger, N. Rockstroh, L. C. Nye, I. Ivanovic-Burmazovic, S. Rau, C. Streb, *Chem. Commun.* **2011**, *47*, 6852 – 6854.
[80] M. Ibrahim, M. H. Dickman, A. Suchopar, U. Kortz, *Inorg. Chem.* **2009**, *48*, 1649 – 1654.
[81] M. Natali, M. Orlandi, S. Berardi, S. Campagna, M. Bonchio, A. Sartorel, F. Scandola, *Inorg. Chem.* **2012**, *51*, 7324 – 7331.
[82] J. Song, Z. Luo, H. M. Zhu, Z. Q. Huang, T. Q. Lian, A. L. Kaledin, D. G. Musaev, S. Lense, K. I. Hardcastle, C. L. Hill, *Inorg. Chim. Acta* **2010**, *363*, 4381 – 4386.
[83] V. A. Grigoriev, D. Cheng, C. L. Hill, I. A. Weinstock, *J. Am. Chem. Soc.* **2001**, *123*, 5292 – 5307.
[84] V. A. Grigoriev, C. L. Hill, I. A. Weinstock, *J. Am. Chem. Soc.* **2000**, *122*, 3544 – 3545.
[85] F. Leroy, P. Miro, J. M. Poblet, C. Bo, J. B. Avalos, *J. Phys. Chem. B* **2008**, *112*, 8591 – 8599.
[86] P. W. Atkins, *Physical Chemistry*, Oxford University Press, **1994**.
[87] S. Kozuch, *WIREs Comput. Mol. Sci.* **2012**, *2*, 795 – 815.

 

[88] Y. Jiang, F. Li, B. B. Zhang, X. N. Li, X. H. Wang, F. Huang, L. C. Sun, *Angew. Chem.* **2013**, *125*, 3482 – 3485; *Angew. Chem. Int. Ed.* **2013**, *52*, 3398 – 3401.
[89] L. L. Duan, C. M. Araujo, M. S. G. Ahlquist, L. C. Sun, *Proc. Natl. Acad. Sci. USA* **2012**, *109*, 15584 – 15588.
[90] M. M. T. Khan, S. A. Mirza, H. C. Bajaj, *J. Mol. Cat.* **1987**, *39*, 323 – 330.
[91] X. López, J. J. Carbo, C. Bo, J. M. Poblet, *Chem. Soc. Rev.* **2012**, *41*, 7537 – 7571.
[92] X. López, P. Miro, J. J. Carbo, A. Rodriguez-Fortea, C. Bo, J. M. Poblet, *Theor. Chem. Acc.* **2011**, *128*, 393 – 404.
[93] J. M. Poblet, X. Lopez, C. Bo, *Chem. Soc. Rev.* **2003**, *32*, 297 – 308.
[94] R. Neumann, C. Abugnim, *J. Am. Chem. Soc.* **1990**, *112*, 6025 – 6031.
[95] B. Chiavarino, R. Cipollini, M. E. Crestoni, S. Fornarini, F. Lanucara, A. Lapi, *J. Am. Chem. Soc.* **2008**, *130*, 3208 – 3217.
[96] J. T. Groves, M. Bonchio, T. Carofiglio, K. Shalyaev, *J. Am. Chem. Soc.* **1996**, *118*, 8961 – 8962.
[97] J. S. Kanady, J. L. Mendoza-Cortes, E. Y. Tsui, R. J. Nielsen, W. A. Goddard, T. Agapie, *J. Am. Chem. Soc.* **2013**, *135*, 1073 – 1082.
[98] K. A. Prokop, H. M. Neu, S. P. de Visser, D. P. Goldberg, *J. Am. Chem. Soc.* **2011**, *133*, 15874 – 15877.
[99] M. S. Seo, J. H. In, S. O. Kim, N. Y. Oh, J. Hong, J. Kim, L. Que, W. Nam, *Angew. Chem.* **2004**, *116*, 2471 – 2474; *Angew. Chem. Int. Ed.* **2004**, *43*, 2417 – 2420.
[100] C. Q. Wang, K. V. Shalyaev, M. Bonchio, T. Carofiglio, J. T. Groves, *Inorg. Chem.* **2006**, *45*, 4769 – 4782.
[101] *Metal-Oxo and Metal-Peroxo Species in Catalytic Oxidations* (Ed.: B. Meunier), Springer, Berlin/Heidelberg, **2000**.
[102] This wave is partially superimposed to a catalytic wave starting above 1600 mV, likely ascribable to water discharge; indeed activity of Ru(DMSO)$PW_{11}$ in water oxidation catalysis with $Ce^{IV}$ as the oxidant has been recently demonstrated.
[103] With respect to the $^{183}W$ NMR spectra of $[(\mu\text{-}O)(Ru^{IV}SiW_{11}O_{39})_2]^{10-}$ reported in ref. 52, 5 signals are observed at the same chemical shift, while the most de-shielded one is found at ca. 60 ppm shift towards higher fields. This may be due to the different counter cation of the species ($Li^+$ in this work, $Cs^+$ in ref. 52). Such effects of the cation on NMR properties are well known for lacunary POMs, see for instance C. Brevard, R. Schimpf, G. Tourne, C. M. Tourney, *J. Am. Chem. Soc.* **1983**, *105*, 7059 – 7063.
[104] J. P. Collman, C. E. Barnes, P. J. Brothers, T. J. Collins, T. Ozawa, J. C. Gallucci, J. A. Ibers, *J. Am. Chem. Soc.* **1984**, *106*, 5151 – 5163.
[105] S. Piccinin, A. Sartorel, G. Aquilanti, A. Goldoni, M. Bonchio, S. Fabris, *Proc. Natl. Acad. Sci. USA* **2013**, *110*, 4917 – 4922.
[106] G. T. te Velde, E. J. Baerends, *J. Comput. Phys.* **1992**, *99*, 84 – 98.
[107] G. T. te Velde, F. M. Bickelhaupt, E. J. Baerends, C. F. Guerra, S. J. A. Van Gisbergen, J. G. Snijders, T. Ziegler, *J. Comput. Chem.* **2001**, *22*, 931 – 967.
[108] A. D. Becke, *Phys. Rev. A* **1988**, *38*, 3098 – 3100.
[109] J. P. Perdew, *Phys. Rev. B* **1986**, *34*, 7406 – 7406.
[110] J. P. Perdew, *Phys. Rev. B* **1986**, *33*, 8822 – 8824.
[111] E. van Lenthe, E. J. Baerends, J. G. Snijders, *J. Chem. Phys.* **1993**, *99*, 4597 – 4610.
[112] E. van Lenthe, E. J. Baerends, J. G. Snijders, *J. Chem. Phys.* **1994**, *101*, 9783 – 9792.
[113] A. Klamt, G. Schuurmann, *J. Chem. Soc. Perkin Trans. 2* **1993**, 799 – 805.
[114] Y. Zhao, D. G. Truhlar, *J. Chem. Phys.* **2006**, *124*, 224105/1 – 6.

Received: June 23, 2014
Published online on August 11, 2014